Numerical Investigation of Design and Operating Parameters of Thermal Gradient Continuous-Flow PCR Microreactor Using One Heater

Authors:

Usama Perwez, Imran Aziz, Faisal Ahmed, Mohsin Raza Khan

Date Submitted: 2020-01-07

Keywords: one heater, PCR kinetics, Lab on Chip (LOC), point-of-care, polymerase chain reaction (PCR), continuous-flow microreactor

Abstract:

To respond to the dire need for miniaturization and process simplification of continuous-flow PCR (CF-PCR) device, this paper represents design and operation guide of a novel metal alloy assisted hybrid microdevice (polydimethylsiloxane (PDMS) and glass) for CF-PCR employing one heater. In this research, the specific objectives are to determine whether one heater chip design will be flexible enough when the size of DNA base pair is varied and to investigate whether one heater CF-PCR device will be able to resolve the longstanding problem of thermal crosstalk. Furthermore, the parametric study is performed to determine which of the fourteen parameters have the greatest impact on the performance of one heater CF-PCR device. The main objective of this parametric study is to distinguish between the parameters that are either critical to the chip performance or can be freely specified. It is found that substrate thickness, flow rate, channel spacing, aspect ratio, channel pass length and external heat transfer coefficient are the most limiting parameters that can either improve or deteriorate the chip's thermal performance. Overall, the impact of design and operating parameters are observed to be least on thermocycling profile at low Reynolds number (?0.37 Re). However, in addition to the primary metric advantages of CF-PCR, one heater chip design helps in minimizing the thermal crosstalk effects by a factor of 4 in comparison to dual heater PCR while still maintaining a critical criteria of chip flexibility in terms of handling various sizes of DNA fragments. Hence, the proposed scheme paves the way for low-cost point-of-care diagnostics, system integration, and device miniaturization, realizing a portable microfluidic device applicable for on-site and direct field uses.

Record Type: Published Article

Submitted To: LAPSE (Living Archive for Process Systems Engineering)

Citation (overall record, always the latest version):	LAPSE:2020.0059
Citation (this specific file, latest version):	LAPSE:2020.0059-1
Citation (this specific file, this version):	LAPSE:2020.0059-1v1

DOI of Published Version: https://doi.org/10.3390/pr7120919

processes

MDPI

Article

Numerical Investigation of Design and Operating Parameters of Thermal Gradient Continuous-Flow PCR Microreactor Using One Heater

Usama Perwez *, Imran Aziz, Faisal Ahmed and Mohsin Raza Khan

Department of Mechanical Engineering, NUST College of Electrical & Mechanical Engineering, National University of Sciences and Technology (NUST), Islamabad P.O. Box 44000, Pakistan; imran_9697@hotmail.com (I.A.); fam.mahesar@gmail.com (F.A.); raza05421@gmail.com (M.R.K.)

* Correspondence: usama13perwez@hotmail.com

Received: 16 September 2019; Accepted: 5 October 2019; Published: 4 December 2019

Abstract: To respond to the dire need for miniaturization and process simplification of continuous-flow PCR (CF-PCR) device, this paper represents design and operation guide of a novel metal alloy assisted hybrid microdevice (polydimethylsiloxane (PDMS) and glass) for CF-PCR employing one heater. In this research, the specific objectives are to determine whether one heater chip design will be flexible enough when the size of DNA base pair is varied and to investigate whether one heater CF-PCR device will be able to resolve the longstanding problem of thermal crosstalk. Furthermore, the parametric study is performed to determine which of the fourteen parameters have the greatest impact on the performance of one heater CF-PCR device. The main objective of this parametric study is to distinguish between the parameters that are either critical to the chip performance or can be freely specified. It is found that substrate thickness, flow rate, channel spacing, aspect ratio, channel pass length and external heat transfer coefficient are the most limiting parameters that can either improve or deteriorate the chip's thermal performance. Overall, the impact of design and operating parameters are observed to be least on thermocycling profile at low Reynolds number (≤0.37 Re). However, in addition to the primary metric advantages of CF-PCR, one heater chip design helps in minimizing the thermal crosstalk effects by a factor of 4 in comparison to dual heater PCR while still maintaining a critical criteria of chip flexibility in terms of handling various sizes of DNA fragments. Hence, the proposed scheme paves the way for low-cost point-of-care diagnostics, system integration, and device miniaturization, realizing a portable microfluidic device applicable for on-site and direct field uses.

Keywords: continuous-flow microreactor; Lab on Chip (LOC), point-of-care; polymerase chain reaction (PCR); PCR kinetics; one heater

1. Introduction

Microfluidic systems have attained enormous recognition in the last two decades due to their characteristics of shortening the reaction time and fast transition within the process. Microfluidic chips have also made significant contributions to many biomedical and genetic related research fields. In microfluidic devices, Polymerase chain reaction (PCR) is a biomedical technique with great potential for on-site evidence collection system of various pathology and food samples. With the invention of polymerase chain reaction (PCR) in 1986 [1], an in-vitro enzymatic amplification of nucleic acid, it has become one of the most appropriate regimes applicable on the microscale biochemical reactions. PCR is one of the most commonly used enzymatic processes that involve discrete thermal cycling, making it a good option to study heat transport characteristics in microfluidic chips. Thermal modeling is a key

element of many biochemical analysis systems, involving operations, such as kinetics analysis [2–4], enzyme catalytic mechanism [5–7], and biochemical interaction analysis [8–10]. Due to lateral thermal diffusion process in microfluidic chips, the thermal profile in microchannel can be accurately captured by using a three-dimensional conjugate heat transfer model.

With rapid advancement in microfluidic technology, the miniaturization of micro-total analysis systems has gained a lot of attention from researchers due to the difficulty in controlling the multiple heaters. The conventional layout of CF-PCR consists of three heaters to produce three discrete temperature zones. However, thermal crosstalk is difficult to avoid in a three heater CF-PCR device. There have been few studies of CF-PCR device using two heaters [11–18]. The main principle behind two step temperature control is to either perform extension and annealing process at same temperature for target amplicons less than 300 base pair (bp) or by creating the extension zone through lateral heat conduction of denaturation and annealing heaters. The thermal management of multiple heaters is one of the constraints for adopting CF-PCR device. To overcome these issues, some researchers have fabricated CF-PCR devices to obtain PCR thermal profile by reducing the number of heaters to one. Wu et al. [19] was the first group to demonstrate one heater CF-PCR device. By stacking multiple layers of polydimethylsiloxane (PDMS) substrate, they obtained two temperature zones by using one heater. In another study, right triangular prism design was realized to fabricate a PDMS based CF-PCR chip [20]. A linear height-dependent temperature gradient was produced on a slanted PDMS surface of chip by utilizing one heater. However, microdevice design and fabrication procedures were complicated for both the chips. Trinh et al. [21] implemented a bent inclination angle concept to fabricate a PDMS-polycarbonate CF-PCR chip. The planar plane of polycarbonate was placed on top of a heater while the bent plane was floating in air. A desired thermal gradient was established with one heater. In another study, Trinh et al. [22] fabricated a novel metal alloy assisted hybrid (PDMS-glass) CF-PCR chip by employing one heater. Invar, high thermal conductivity metal alloy, was sandwiched between the chip and the heater to establish a thermal gradient on the chip. By varying the protrusion length of the invar sheet, different thermal zones can be established on the chip. Chen et al. [23] incorporated heat pipes as a cooling system with one heater to build a CF-PCR chip. The heater was integrated to the center of the chip while two heat pipes with a fan were placed on the opposite sides of the chip to produce five temperature zones on it. The unique concept utilized in this study is well applied for a low-cost PCR system.

Although microfluidics has exhibited the potential to miniaturize and simplify many laboratory routines, an essential comprehension of the thermofluidic modeling tools is ultimately critical to streamline the design process of microfluidic device. One of the main obstacles for device miniaturization and process simplification of continuous-flow PCR (CF-PCR) device is employing two or more heaters which leads to process complexity. To overcome these complexities, a novel metal alloy assisted hybrid microdevice (polydimethylsiloxane (PDMS) and glass) for CF-PCR employing one heater is considered. In this paper, we perform three-dimensional thermal modeling of a planar hybrid PDMS-glass microfluidic device employing a single heater. This concept employs relatively high thermal conductivity material (invar) to create two discrete temperatures when invar sheet made partial contact with the heater and rest of the sheet is exposed to air. The specific objectives of this study are as follows: (a) To determine whether one heater chip design will be flexible enough when the size of DNA base pair is varied, (b) To investigate whether one heater CF-PCR device will be able to resolve the longstanding problem of thermal crosstalk or not, and (c) To evaluate the effect of design, flow, and external parameters on the thermal performance of one heater CF-PCR device. The initial segment of this paper illustrates the design and mathematical model of a microfluidic reactor. The following section provides the validation and verification of the model in terms of temperature data, residence time, and DNA amplification efficiency. The third section discusses the numerical results of a one heater planar CF-PCR device.

2. Description of CF-PCR Microfluidic Chip

2.1. Design of Microfluidic Chip

CF-PCR device presented in the current study consists of three parts: (a) PCR chip, through which sample flows, (b) an invar sheet sandwiched between the microfluidic chip and heater, and (c) a hot aluminum plate for temperature distribution regime on a chip. The design of CF-PCR follows the concept of a metal alloy assisted planar microdevice using serpentine microchannel as proposed by Trinh et al. [22]. Figure 1a shows the top view of the hybrid CF-PCR microdevice whose size is 75 mm × 50 mm. A planar microdevice has been built by permanently bonding 1 mm thick glass (δg) with 3 mm thick cover layer of PDMS (δp). Geometry of the invar sheet is based on the variations of the protrusion length. The protrusion lengths of 3, 4, and 5 cm are used to tune the temperature zones depending upon the DNA template size. A hot aluminum plate (180 mm × 180 mm) is used to create the specific temperature gradients on the hybrid CF-PCR chip.

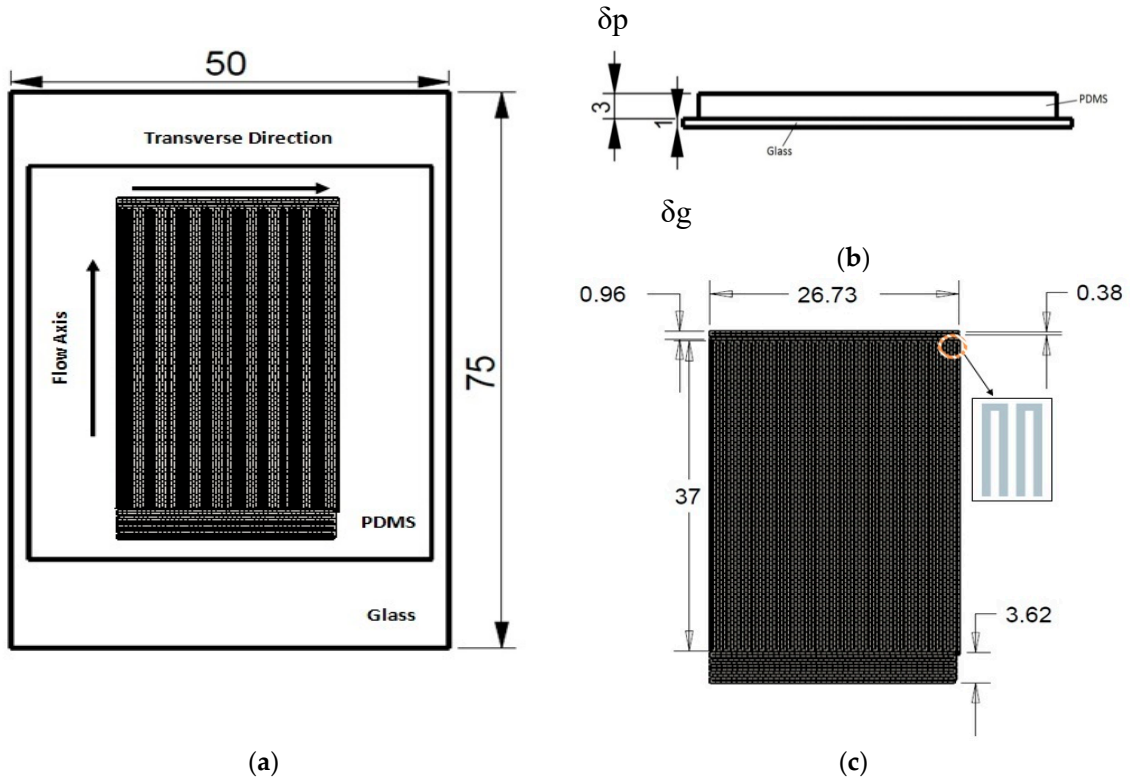

Figure 1. Design of the microfluidic device: (**a**) top view of the CF-PCR microfluidic device; (**b**) cross section of the device (dimensions in mm); (**c**) A 32-thermal cycle serpentine microchannel (dimensions in mm).

2.2. Design of Microfluidic Microchannel

The geometrical characteristics of the microfluidic channel greatly affect the thermal performance of the device. In order to achieve better DNA amplification, 18–40 thermal cycle loops are generally required. The dimensions of serpentine microchannel for 32 cycles are shown in Figure 1c for which the width is 200 μm, height is 75 μm with total length of 2.7 m. However, DNA amplification efficiency depends on the PCR protocol which is defined by the residence time per cycle in each zone. Typically, residence time for the extension zone is higher than that for the other two zones. The PCR protocols of

1:1:2 or 1:1:3 (denaturation, annealing, and extension residence time per cycle) are commonly used. The average residence time (t) in a channel is given by:

$$t = \frac{L \times w \times h}{Q} \quad (1)$$

where L, w and h are the length, width, and height of the microchannel; and Q is the volumetric flow rate. The head loss of the channel needs to be examined to understand the acceptable pressure loss required for chip operation. The maximum allowable pressure loss for glass-PDMS bonding to withstand is 200 kPa. The pressure loss is basically an important parameter which constraints the maximum flow rate within the channel. The pressure loss (p) within serpentine microchannel is given by [24]:

$$\Delta P = f\frac{L}{D_h}\rho\frac{V_{avg}^2}{2} + k_b\,\rho\frac{V_{avg}^2}{2} \quad (2)$$

where V_{avg}, ρ and k_b are the fluid average velocity, density and bend loss coefficient.

3. Mathematical Model and Numerical Methods

3.1. Governing Equations

A simplified two-dimensional heat transfer model is presented to identify the critical factors affecting temperature regime in a microfluidic flow channel (see Figure 2a). The control volume analysis in channel across length Δx is given by:

$$A_i\rho_f V_{avg} Cp_f\frac{dT(x)}{dx} - A_i k_f\frac{d^2T(x)}{dx^2} + (h_I(x))b(T(x) - T_\infty) = q_i''(x)(1-\alpha_i)b \quad (3)$$

where A_i is the cross-sectional area of the fluid channel, Cp_f is the specific heat capacity of the fluid, T(x) is the temperature of the fluid, $h_I(x)$ is the effective heat transfer coefficient from the surface of fluid channel, $q_i''(x)$ is the heat flux from heater, and α_i is the heat loss factor. The α_i accounts for the unmodeled heat loss through invar and glass substrate. The effective heat transfer coefficient depends on the substrate thickness (δ), substrate properties (k) and external environment conditions (h_{air} = 15 W/m^{2}k). The $h_I(x)$ is determined empirically by using one-dimensional heat transfer model as:

$$\frac{1}{h_{eff}} = \frac{1}{h_{air}} + \frac{\delta}{k} \quad (4)$$

The two-dimensional model shows that the local fluid temperature is a function of microchannel geometry, heat flux, heat transfer coefficients from the top surface of the fluid channel, and heat loss factors. The limitation of the two-dimensional heat transfer model is the unaccounted three-dimensional thermal diffusion which occurs in the fluid channel and substrates (PDMS, glass, and invar) as well as the natural convection to air. To develop exact thermal profile of PCR chip, a three-dimensional conjugate heat transfer model is required. A three-dimensional simulation model for PCR chip is complemented by heat transfer equation in the solid and fluid domain as:

$$\rho C_p\frac{dT}{dt} + \rho C_{pf}\boldsymbol{u}.\nabla T = \nabla.(k\nabla T) + Q_j \quad (5)$$

where T is temperature, Q_j is the heat generation rate of heater, C_{pf} is the specific heat capacity and ρ is the density. The assumptions of three-dimensional heat transfer model are consideration of transient and thermal diffusion terms only inside substrates (PDMS, glass, and invar) and ignoring the viscous dissipation term in fluid domain. Heat generation rate of heater is fundamentally presented by joule

heating which produce desired temperature regimes by applying current density at the inlet while the outlet is grounded. The heat generation rate in terms of the Joule heating is given by:

$$Q_j = J_j.E_j \tag{6}$$

where J_j is the current density and E_j is the electric field at heater j. The heat generation rate is zero except for the only heating element. The heat generation rate is adjusted to achieve the desired temperature requirement in the denaturation zone. The convection-diffusion species transport model is presented by an equation as below:

$$\frac{dC_i}{dt} + \nabla.(-D_i \nabla C_i) + \boldsymbol{u}.\nabla C_i = R_i \tag{7}$$

where D_i and C_i are the mass diffusivity coefficient and concentration of the species. R_i is a source term which is the net output rate of species and defined by the PCR reaction kinetics.

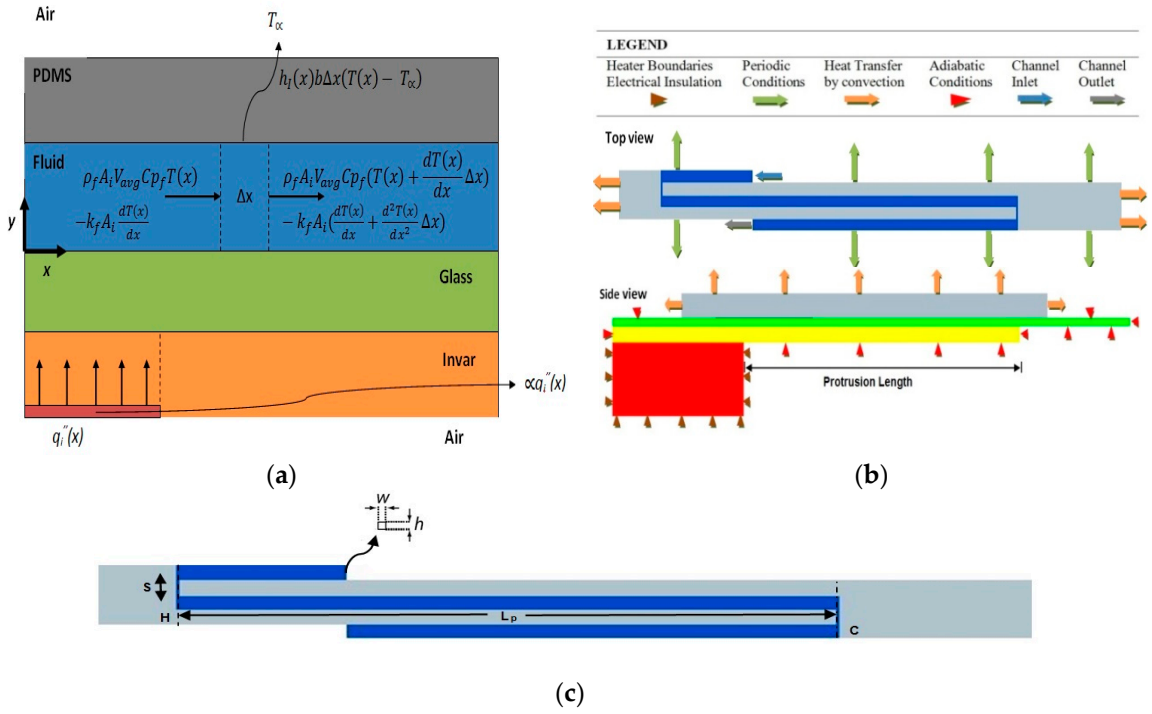

Figure 2. Boundary conditions visualization: (**a**) simplified two-dimensional control volume analysis in the microchannel; (**b**) one-cycle computational model; (**c**) overview of microchannel design parameters.

3.2. Computational Model

A hybrid (PDMS-Glass-Invar) thermal gradient CF-PCR device employing one heater is simulated in ANSYS CFX 15 [25], a commercial finite-volume solver package. DNA injected in the fluid channel moves toward the single heater and denaturation occurs at first channel bend. Subsequently, fluid cools as it passes through the appropriate temperature gradient established by invar without any specific heater and annealing of single-stranded DNA occurs as it approaches second channel bend. In the final step, DNA extension occurs as fluid moves towards the single heater in the next straight channel zone and the process then repeats itself. The output metrics for this study are based on the criteria of achieving requisite temperature profile that is compatible with most of the PCR applications. The successful annealing, extension, and denaturation are defined to occur in the temperature ranges of 328–338 K, 343–348 K, and 363–369 K, respectively [26]. Convergence criteria of 0.01 K for temperature field is used in the mesh refinement study. For all simulations, the solution is considered to be

converged when the residuals of continuity, momentum, and energy equations for all variables are less than 10^{-6}. Table 1 shows nominal parameters based on the chip design of Trinh et al. [22] and the chip parameters that are studied for different ranges in this work.

Table 1. Variation of chip design and operational parameters (bold presents nominal parameters).

Parameter	Value Range
Substrate thickness	**1**, 2, and 3 mm
Chip cover thickness	1, 2, and **3** mm
Metal alloy thickness	**0.5**, 1, and 1.5 mm
Substrate-cover material	**Glass**, **PDMS**, silicon, and hybrid combination
Inlet/Outlet location	Hot, cold, and **mid** temperature
Channel spacing (s)	**0.38**, 1, 2, and 5 mm
Aspect ratio (h/w)	0.09, 0.16, **0.37**, and 1.5
Protrusion length	3, **4**, and 5 cm
Pass length (L_p)	30, **37**, and 45 mm
External heat transfer coefficient ($\bar{h}$)	5, 10, **12**, and 15 W/m^{2}K
Ambient Temperature (T_α)	288, 293, **298**, and 303 K
Reynolds number (Re)	0.06, 0.12, **0.27**, 0.37, 0.61, 1.14, and 2.46

In the first step, solid domain simulation model is developed to validate the experimental results. This model incorporates the assumption of neglecting fluid domain which results in difference between numerical and experimental thermal profile due to two reasons: (1) different thermal conductivity of water and PDMS, and (2) neglecting the convective heat transfer induced by the fluid flow within the microchannel. Using the equation $\delta_i \Delta k/(\delta_p k_p)$, the percentage change in the thermalresistance is less than 0.61%. Hence, the thermal profile relative to one-cycle model would differ by less than 0.31 K. Despite the inaccuracies induced by the exclusion of fluid flow, the solid domain model contains the attributes necessary to estimate the chip-wide temperature variance through the microfluidic device. The boundary conditions applied to solid domain model are as follows:

i. All top and side walls of PDMS are imposed with natural convective boundary conditions. The value of external heat transfer coefficient ($\bar{h}$) is estimated by using empirical relation of Nusselt number and Rayleigh number as [24]:

$$Nu = \frac{hL_c}{k_{air}} = 0.54Ra^{1/4},\ Ra = \frac{g\beta\Delta TL^3Pr}{\nu^3} \quad (8)$$

where g is gravity, β is the coefficient of thermal expansion, Pr is prandtl number and ν is the kinematic viscosity. The external heat transfer coefficient is 12 W/m^{2}K in our study.

ii. All walls of glass and invar have adiabatic boundary conditions due to black insulating tape.

iii. Joule heating is incorporated within the model by applying uniform current density at the inlet of the hot plate while outlet of the hot plate is grounded. The input voltage of 0.0785 V is estimated through numerical experimentation to achieve the desired temperature requirement in denaturation zone (the heat generation rate of 7.18×104 W/m^3).

iv. Radiation effects are not considered due to negligible effect on the heat transfer model.

v. Isotropic properties are assumed for PDMS, glass, and invar. The thermal properties of PDMS, glass, invar, silicon, and aluminium used in the simulations are listed in Table 2.

Table 2. Material properties.

Material	p (kg/m^3)	k (W/m K)	C_p (J/Kg K)
Glass	2230	1.1	753
PDMS	0.97	0.15	1460
Silicon	2330	141.2	700
Invar	8055	10	515
Aluminum	2700	247	903

In the second step, one-cycle computational model is developed using periodic boundary conditions. The total length (along the flow direction) of the one-cycle model is 75 mm and the width (along the transverse direction) is 1.38 mm. The one-cycle computational model of the hybrid (PDMS-Glass-Invar) PCR chip with appropriate boundary conditions are shown in Figure 2b. The boundary conditions, including solid domain, applied to one pass model are as follows:

i. Periodic boundary conditions are imposed on the side walls of PDMS, glass, and invar.
ii. Inlet fluid velocity and temperature are specified at the inlet of the channel. Inlet fluid temperature is assumed equal to no flow substrate isotherm.
iii. Outlet boundary condition of zero-gauge pressure is considered.
iv. Temperature dependent properties of water, a working fluid, are incorporated within the channel domain.
v. Species concentration are calculated by considering outlet concentration profile of cycle i at the inlet of cycle $i + 1$.

3.3. PCR Kinetics Model

PCR DNA amplification is a very complex process with handful of details are available for chemical reactions that are involved in three steps of PCR. The PCR kinetic model adopted in this study to formulate and estimate kinetic parameters is proposed by Hunicke-Smith [27–29]. The chemistry model consists of five major chemical species which control the reactions in denaturation, annealing, and extension zones. The first chemical reaction represents splitting of S_1S_2 (double-stranded DNA (dsDNA)) into S_1 and S_2 (single-stranded DNA (ssDNA)).In the second and third chemical reactions, P_1 and P_2 (forward and reverse primers) bind on ssDNA to form primer-ssDNA complexes (S_1P_2 and P_1S_2). The fourth and fifth chemical reactions denote the extension stage of PCR DNA process (Table 3). The forward and backward reaction rate constants are basically dependent on temperature. The reaction rate constants expressions are basically temperature dependent, which are given as follow:

$$K_D^+(T) = \frac{K_0^+\left(1 + \tanh\left[\frac{T-88}{5}\right]\right)}{2} \tag{9}$$

$$K_D^-(T) = \frac{K_0^-\left(1 + \tanh\left[\frac{-(T-75)}{5}\right]\right)}{2} \tag{10}$$

$$K_A^+(T) = \frac{K_1^+\left(1 + \tanh\left[\frac{-(T-62.5)}{5}\right]\right)}{2} \tag{11}$$

$$K_A^-(T) = \frac{K_1^-\left(1 + \tanh\left[\frac{T-66)}{5}\right]\right)}{2} \tag{12}$$

$$K_E(T) = K_2 \exp(-\left[\frac{T-72}{5}\right]^2) \tag{13}$$

where T is the fluid temperature in °C and $k_0{}^+$, $k_0{}^-$, $k_1{}^+$, $k_1{}^-$, and k_2 are equal to 12.5 s^{-1}, 10^9 M^{-1} s^{-1}, 5 $\times$ 10^9 M^{-1} s^{-1}, 10^{-4} s^{-1}, and 0.32 s^{-1}, respectively. The operational parameters, initial concentration and diffusion coefficient, of the species are given in Table 4 [30].

Table 3. List of all reactions in real-time PCR.

Step	Reaction
Denaturation	$S_1S_2 \underset{K_D^-}{\overset{K_D^+}{\leftrightarrow}} S_1 + S_2$
Annealing	$S_1 + P_2 \underset{K_A^-}{\overset{K_A^+}{\leftrightarrow}} S_1P_2$
	$S_2 + P_1 \underset{K_A^-}{\overset{K_A^+}{\leftrightarrow}} P_1S_2$
Extension	$S_1P_2 \rightarrow k_E S_1S_2$
	$P_1S_2 \rightarrow k_E S_1S_2$

Table 4. Operational parameters of the species.

Species	Initial Concentration (mol/m^3)	Diffusion Coefficient (m^2/s)
$S_1$and S_2	0	10^{-10}
P_1 and P_2	3×10^{-7}	10^{-9}
S_1P_2 and P_1S_2	0	10^{-10}
S_1S_2	5.71×10^{-12}	10^{-10}

3.4. Mesh Sensitivity Analysis

In the first step, the grid independence analysis is carried out for the solid domain model by varying the grid density in three-dimensional model. Hexahedral meshing scheme of uniform size is used to mesh the solid domain model due to large difference in substrates thickness (Figure 3a). The complexity of the model is reduced by excluding fluid domain. The number of meshing elements are varied from 0.01 million to 3.75 million, and the absolute error of the temperature is specified as a criteria to ensure that results are independent of the hexahedral meshing scheme. A specific point in the domain is chosen for performing the grid independence analysis; x = 25 mm, y = 37.5 mm, and z = 2.25 mm. The temperature obtained in PDMS-glass-invar heat transfer model is shown in Figure 3b for seven different grid sizes to analyze the effect of grid density. It is observed that the variations in the grid refinement result in absolute error less than 0.91 K. Hence the grid size consisting of 1.87 million elements is chosen for this study.

In the second step, mesh refinement of one-cycle computational model is performed to have good grid density quality. In one-cycle computational model, there are three domains: (i) glass-invar-heater, (ii) PDMS, and (iii) fluid domain. For each domain, the grid density is increased by keeping other domains constant. In the fluid domain, mesh points are varied along the length, width, and height within microchannel to analyse the velocity profile. Figure 3c shows the velocity profile in transverse and streamwise direction. It is observed that the velocity profiles within a microchannel are parabolic and blunt in streamwise and transverse direction respectively. As per basic concept of microfluidics, blunt velocity profile in transverse direction is due to lower aspect ratio of rectangular microchannel than 0.4 [31]. In other two domains, refinement of grid density results in decrease of the absolute error slope. It is also observed that further increase of number of elements has marginal improvement in the error discrepancies of the model. Hence, one-cycle computational model consists of 3.03 million mesh elements.

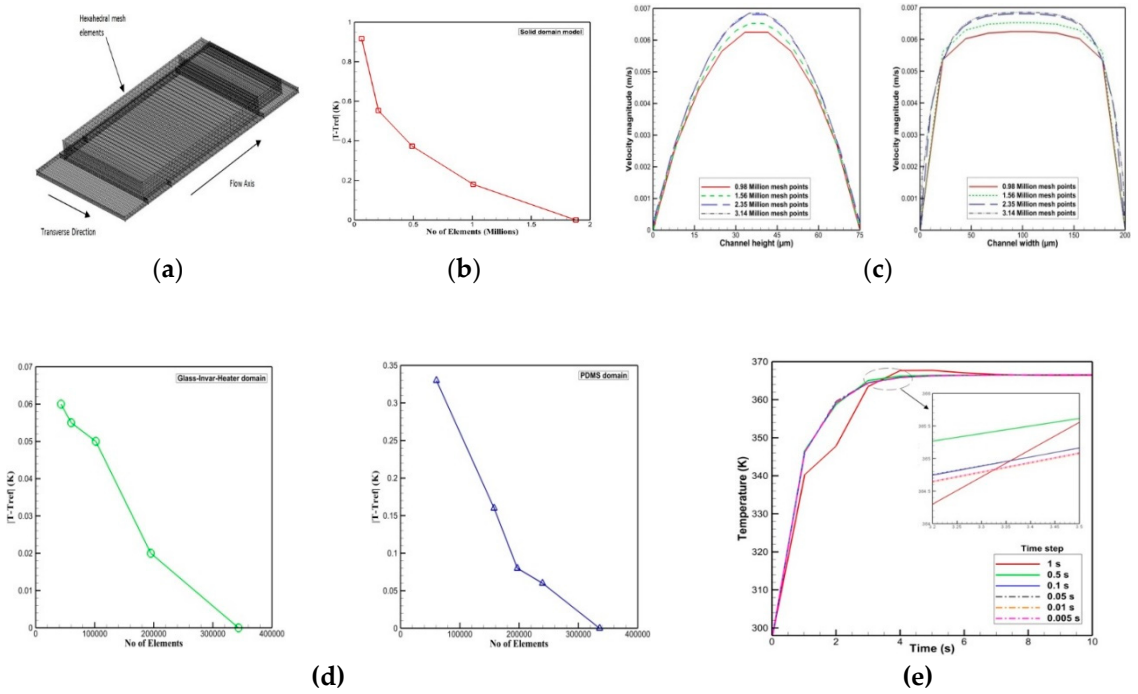

Figure 3. (**a**) Meshing of the solid simulation model (PDMS-glass); effect of grid density on: (**b**) solid domain model; (**c**) velocity profile in microchannel (along height and width) and (**d**) one-cycle model (glass-invar-heater domain and PDMS domain); (**e**) time-step independence analysis of maximum temperature in one-cycle model.

3.5. Time-Step Sensitivity Analysis

Time-step independence test is performed using time-steps of 1, 0.5, 0.1, 0.05, 0.01, and 0.005 s as shown in Figure 3c. Temperature distribution in different zones is a very critical factor in PCR DNA process. Hence, temperature distribution response needs to be maintained at constant level in the denaturation zone. The adequate thermal controller response can be achieved by ensuring small time-step. A time-step of 0.01 s is found to provide the accurate thermal response of the chip system.

3.6. Model Validation

The numerical model presented in this study is compared with Trinh et al. [22] findings to validate temperature gradient on glass substrate in a one heater flow-through PCR device. Trinh et al. [22] experimentally examined 3, 4, and 5 cm protrusion length (relative to heater) of invar, a relatively higher thermal conductive material, by sandwiching it between a planar hybrid PDMS-glass microfluidic device and single heater. The heater in contact with invar sheet was maintained at 368 K, and the sample injected in the microchannel was controlled at the flow rate of 2 μL min^{-1} (or 0.27 Re). The deviation of temperature gradient between the experimental and numerical results are less than 1 K. This shows that the present numerical scheme can accurately predict the thermal performance of CF-PCR chip using one heater. It is also observed that increase in protrusion length provides a larger temperature gradient (ΔT) across the substrate. In terms of comparison of various protrusion length, the thermal profile of 3 and 5 cm protrusion length configurations are not compatible with the requisite PCR temperature regimes in annealing and denaturation zones respectively as shown in Figure 4. Thus, the 4 cm protrusion length configuration is chosen to perform further simulations to investigate the thermal performance of one heater CF-PCR chip.

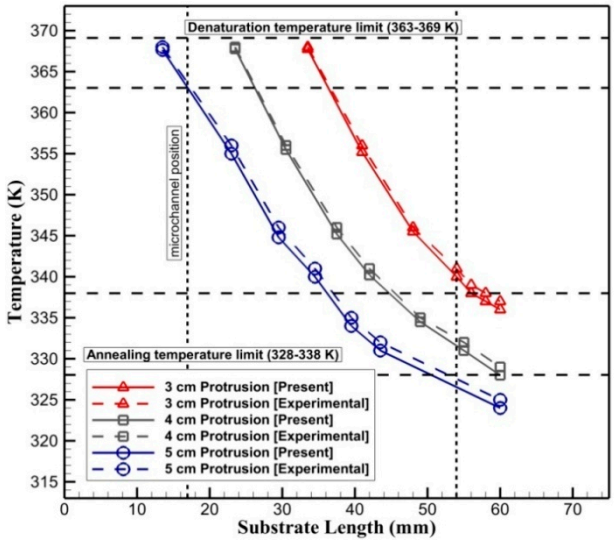

Figure 4. Comparison of temperature profiles on glass surface with experimental data for various protrusion length of invar.

4. Results and Discussion

4.1. Chip Design Parameters

4.1.1. Substrate-Cover Material

In CF-PCR system, silicon, glass, PDMS or hybrid stack are commonly utilized as substrate materials. In our study, substrate-cover materials of glass, glass-PDMS, glass-silicon, PDMS, PDMS-glass, silicon, and silicon-glass are investigated. The effect of thermal conductivity (k) is most relevant in terms of thermal properties as shown in Table 2. It is generally considered that increase in thermal conductivity results in: (1) increase of conduction effects throughout material, (2) decrease of nonlinearity effects in substrate temperature gradient, and (3) higher overall system temperature. The influence of various substrate-cover materials on temperature profiles along longitudinal direction is given in Figure 5a. It is observed that denaturation temperature for PDMS, the least thermal conductive material, is below acceptable temperature regime by 4 K, while annealing and extension temperatures for silicon, the most thermal conductive material, are above acceptable temperature regime by 40–50 K. It shows a very significant variation of temperature from allowable thermal protocols in various regions for PDMS and silicon. However, with some adjustment of heater temperature for PDMS, acceptable limits can be achieved, but it will yield effects of thermal expansion and substrate degradation near 450 K. In a hybrid stack configuration, silicon as either substrate or chip cover cannot be successfully implemented, while PDMS is an excellent option as a chip cover due to lower-k material (minimum convection effects) as observed in glass-PDMS temperature profile. The use of glass or glass-PDMS demonstrated acceptable chip-wide temperature variance. Thus, it is anticipated that substrate-cover material needs to be selected carefully, and glass or glass-PDMS is an excellent substrate-cover material choice for one heater chip, which can lead to the additional benefits of low-cost and commercially viable point-of-care diagnostics.

4.1.2. Substrate Thickness

Glass-PDMS substrate is most commonly used in microfluidic system due to compatible combination, low material cost, and commercial availability. Taguchi method is employed to investigate the effect of glass-PDMS thickness variation on temperature distribution. Taguchi method is a robust product design tool used to optimize design of experiment statistically. In Taguchi method, a special set of arrays, orthogonal arrays, are used to arrange critical design parameters. This method lists the

number of parameter combinations required for the experiment that help in reducing the number of experiments needed for gauging overall system performance. In this study, three parameters and levels are considered. Table 5 presents three parameters that are subjected to study: metal alloy thickness (invar), substrate thickness (glass), and cover thickness (PDMS). The chosen parameters are investigated to obtain optimized substrate thickness for one heater CF-PCR chip. Table 6 shows nine sets of parameter combinations that are required to define $L_9(3^3)$ orthogonal array. This reduces the number of parameter combinations to 9, otherwise it would have been 27 (3^3) combinations.

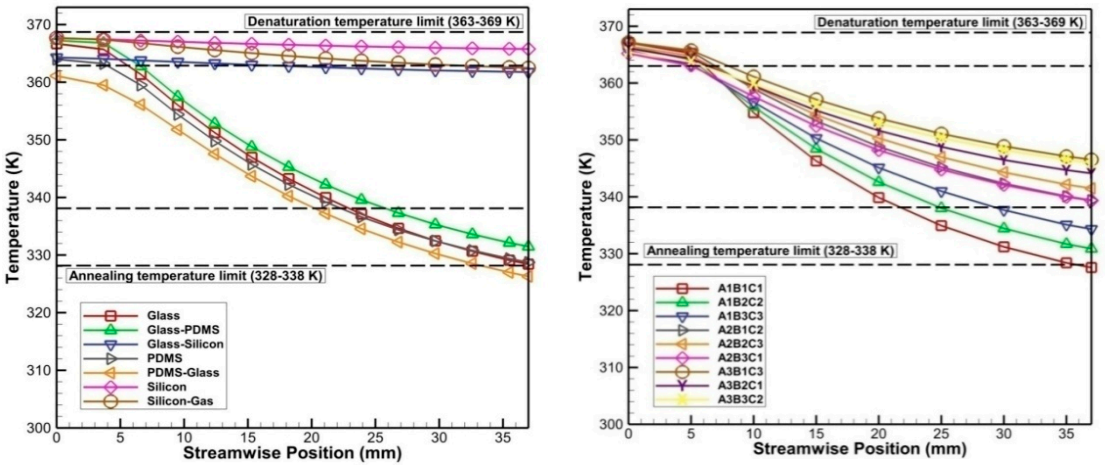

Figure 5. Variation of temperature profiles along the streamwise position in the microchannel: (**a**) substrate-cover materials; (**b**) substrate thickness.

Table 5. Parameters used for Taguchi method.

No	Parameter	1	2	3
A	Metal alloy thickness (mm)	0.5	1	1.5
B	Substrate thickness (mm)	1	2	3
C	Cover thickness (mm)	1	2	3

Table 6. $L_9(3^3)$ orthogonal array of the Taguchi method.

Case No	A	B	C
1	1	1	1
2	1	2	2
3	1	3	3
4	2	1	2
5	2	2	3
6	2	3	1
7	3	1	3
8	3	2	1
9	3	3	2

Figure 5b shows temperature distribution along the streamwise position obtained from simulations with nine sets of thickness parameters. With increase of metal alloy (invar) thickness, temperature profiles start to fall above acceptable thermal protocol due to relative enhancement of heat rates across annealing and extension regions. Thus, it is obvious that as metal alloy thickness varies, heating rates become more significant, which results in steeper temperature profiles. Conversely, the temperature variance in denaturation region is nearly flat with maximum difference of 1.5 K. This suggests that increasing the heater temperature can be used to attain acceptable denaturation temperature

limits. Additionally, it is also observed that temperatures do not vary linearly or consistently with substrate-cover (or glass-PDMS) thickness variation due to a complex conjugate three-dimensional heat transfer phenomena. The longitudinal-wise temperature variance is nearly doubled, from approximately 19 K for the A3B3C2 set parameter to 39 K for the A1B1C1 set parameter. This lesser longitudinal-wise temperature variance for 1.5-mm thick invar assisted chip is in accordance with the increase of lateral heat rates, which leads to undesirable PCR temperature limits while using one heater chip. For 0.5-mm thick invar assisted chips, all temperature profiles are well withinthe acceptable annealing temperature limit (328–338 K). This indicates that the variation of metal alloy thickness adversely affects the thermal profile and needs to be selected carefully for obtaining acceptable PCR protocols. Hence, it is anticipated that a one heater hybrid device of glass-PDMS substrate can only yield desire PCR amplification with thinner (or 0.5-mm thick) metal alloy substrate.

4.1.3. Inlet/Outlet Location

In general, inlet/outlet locations are mostly process flexible depending on the specified on-chip feature. Mostly, hot inlet/outlet locations are proposed to ensure that initial sample attains complete denaturation without any degradation. Mid inlet/locations are preferred when double-stranded DNA (dsDNA) are required as output. The effect of inlet/outlet locations on maximum fluid temperature in denaturation region and minimum fluid temperature in annealing region are investigated. In this study, three inlet/outlet locations, hot, cold, and mid, are considered based on their position relative to channel bends. A hot inlet/outlet location is located on line H, which aligns with denaturation bend. A cold inlet/outlet location is located on line C, which aligns with annealing bend, while a mid-inlet/outlet location is between the two positions as shown in Figure 2c. It is to be noted that with increase of Reynolds number (Re), the inlet/outlet locations minimally affect the maximum fluid temperature in denaturation region. Thus, the maximum variance in fluid denaturation temperature is 0.7 K with the variation of inlet/outlet configurations as shown in Figure 6a. The significant impact of inlet/outlet locations on minimum annealing temperature is supported by the variation of mean temperature fluid (T_m) in flow direction x when maintained at constant surface temperature (T_s) is given by:

$$T_m(x) = T_s - (T_s - T_i)\exp\left(\frac{-hp}{\dot{m}C_p}x\right) \tag{14}$$

where T_i is the initial temperature of the fluid, $\dot{m}$ is the mass flow rate and p is the perimeter of rectangular microchannel. This shows that the higher the mass flow rate, the bigger the distance required to achieve the temperature change. Thus, the maximum variance in fluid annealing temperature is 7.43 K with variation of inlet/outlet configurations as shown in Figure 6b. In contrast to the above observation, the negligible effects of cold inlet/outlet location on annealing temperature are given by axial heat conduction in direction x as:

$$Q_s'' = K_s\left(\frac{T_{s,i} - T_{s,i+1}}{\Delta x}\right) \tag{15}$$

where $T_{s,i}$ is the average solid temperature at first section and $T_{s,i+1}$ at the next section. It is important to note that axial heat conduction is the main term which tends to reduce variance and flatten the annealing temperature even with increase of Reynolds number due to alignment of both inlet and outlet along line C. A similar argument can be constructed for the effect of hot inlet/outlet location on denaturation temperature. However, any location of inlet/outlet location between hot and cold configuration can be freely specified for one heater PCR if Reynolds number is less than 0.62 because temperature variance is less than 1 K for both cases.

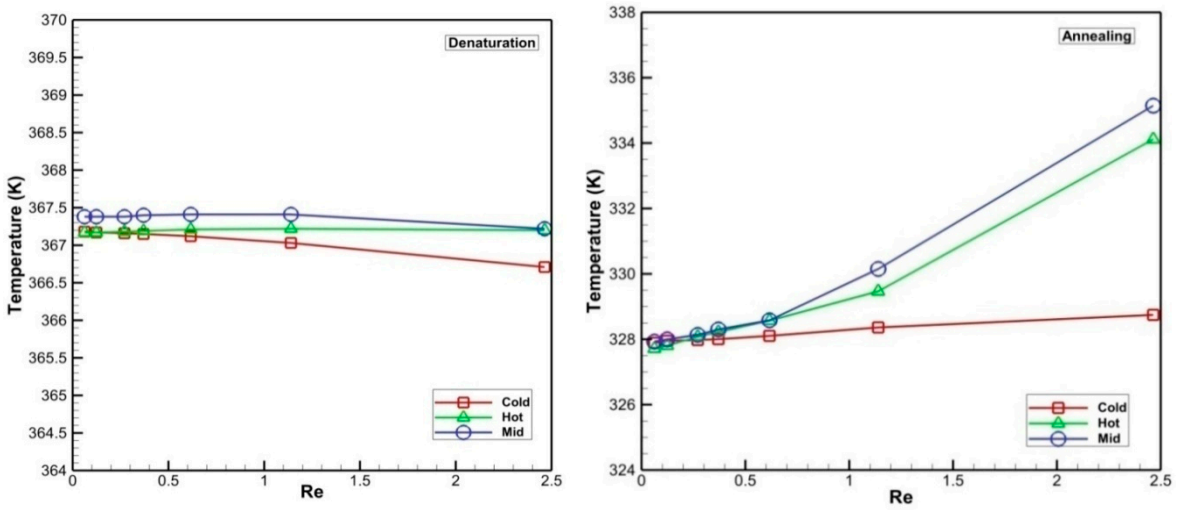

Figure 6. Effect of Reynolds number (Re) for various inlet/outlet locations: (**a**) maximum denaturation temperature; (**b**) minimum annealing temperature.

4.1.4. Channel Spacing (s)

In microchannel, channel spacing less than 100 μm is difficult to fabricate and results in more chip width with the increase of channel spacing [32]. In practice, channel spacing affects chip size which is a major design constraint for miniaturization of microfluidic device. This is, of course, a design trade-off between the channel spacing and the chip size. For an optimum microchannel design, the channel spacing should be selected in a way to minimize the chip width while achieving the desired temperature gradient. The channel spacing of 0.38, 1, 2, and 5 mm are investigated in this study. It is observed that increasing the channel spacing results in higher temperature at denaturation bend because of a straight channel section adjacent and parallel to heating configuration. Thus, it is obvious that as channel spacing increases, fluid more closely approaches the heater temperature. In contrast to the above observation, fluid experiences lesser cooling due to influence of natural convection phenomena at annealing bend rather than the convective heat rate. However, the increase of Reynolds number decreases temperature uniformity in channel bends due to flow maldistribution. This also suggests that temperature uniformity in a specific channel spacing region is highly sensitive to flow rate (or Reynolds number). It is to be noted that temperature uniformity incorporation due to channel spacing is related to more residence time along heating/cooling configuration rather than influence of axial heat conduction within adjacent channels.

The effect of channel spacing on temperature profile is significant as shown in Figure 7a. In general, we expect increase in channel spacing to result in increase of temperature gradient (ΔT). However, the results indicate that this is indeed not the case for one heater CF-PCR chip. Short channel spacings (≤1 mm) attain greater temperature gradient across the chip, but the variable throughput leads to variance of temperature gradient (ΔT) while remaining well within the temperature limits (a variance of 7.36 K for a 0.38 mm spacing). Conversely, long channel spacings result in undesirable chip-wide temperature gradient, but as expected, it leads to more consistent temperature gradient (ΔT) across the chip even at higher Reynolds number (≤0.6 K variance for a 5 mm spacing). This indicates that the adjustment of channel spacing leads to a trade-off between desirable chip-wide temperature gradient and uniformity of temperature gradient. Overall, this is an important result indicating that in the absence of other design considerations, short channel spacings (≤1 mm) are recommended.

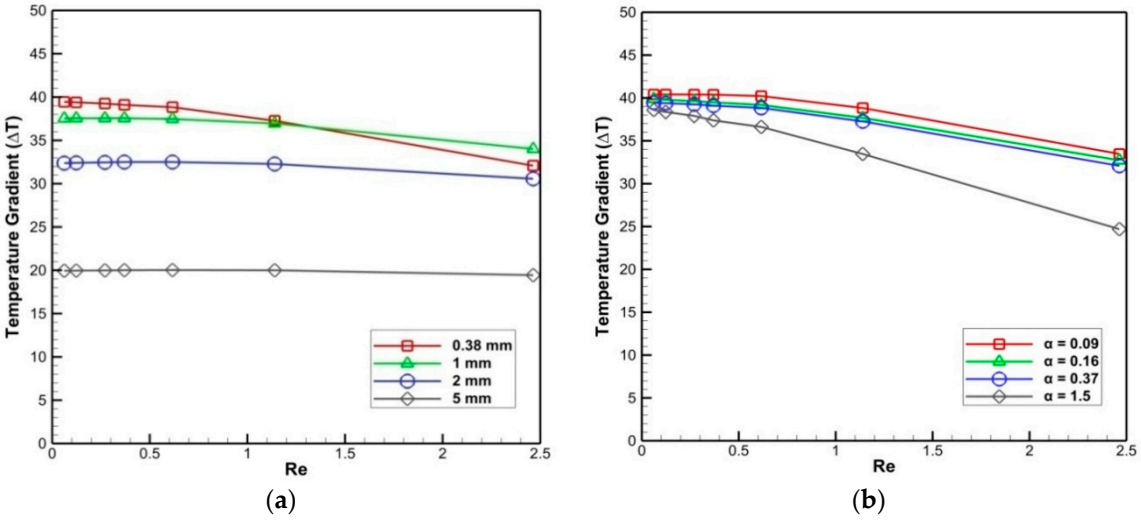

Figure 7. Effect of Reynolds number (Re) on temperature gradientacross the chip due to: (**a**) channel spacing; (**b**) aspect ratio.

4.1.5. Channel Aspect Ratio (α)

In common design approach for microfluidic PCR platform, channel aspect ratio of microchannel is mostly varied between 0.1 to 1. In practice, channel aspect ratio affects residence time which is a major constraint for rapid PCR device. This is, of course, a trade-off between the channel aspect ratio and the residence time. Thus, channel aspect ratio of 0.09, 0.16, 0.37, and 1.5 are investigated to study the realistic channel geometry variations using one heater configuration (Table 7). Channel aspect ratio is defined as the ratio of channel depth to channel width (h/w). In this study, channel aspect ratios are varied while maintaining constant channel cross-sectional area at 0.015 mm^2.

Table 7. Channel aspect ratios used in parametric study.

Aspect Ratio	h (mm)	w (mm)	One Cycle Width (mm)
0.093	0.0375	0.4	1.96
0.167	0.05	0.3	1.46
0.375	0.075	0.2	0.96
1.5	0.15	0.1	0.66

It is observed that channel aspect ratio minimally affects denaturation temperature, which varies by less than 0.7 K. Although with the variation of flow rate, it results in negligible effect of aspect ratio on denaturation temperature that is governed by convective heat rate equation for fully developed laminar flow in a straight tube with an isoflux boundary condition as shown in Equation (16).

$$q'wall = \frac{1}{8}NuQ\rho cp\ \frac{dT}{dx} \tag{16}$$

where q'_{wall} is the convective heat rate, Nu is the Nusselt number, and dT/dx is the axial temperature gradient of the fluid. This shows that the convective heat rate is proportionally dependent on volumetric flow rate and axial temperature gradient. It is obvious that at constant volumetric flow rate, higher convective heat rate will result in higher axial temperature gradient. However, the significant effect of aspect ratio on annealing temperature with increase of flow rate is supported by Equation (14), and the axial heat conduction between adjacent channels that is related to conductive resistance depends on channel spacing and thermal conductivity of substrate (R_{cond} = s/k). As per Equation (14), the higher the mass flow rate or channel cross-sectional area is, the bigger the distance required to achieve the temperature change. Thus, a microchannel with smaller height is feasible for faster fluid temperature

change at a given mass flow rate. Table 7 indicates that channel height is being increased with the increase of channel aspect ratio. This is one of the contributing factors that result in smaller axial temperature gradient. Meanwhile, channel spacing also reduced with the increase of channel aspect ratio and that causes increase of axial heat conduction on fluid temperature change at a particular location. Additionally, in microfluidic systems, axial heat conduction will be a significant factor if axial temperature gradient is in the order of 1 °C/mm [24]. As mentioned above, this coupled phenomena affects temperature distribution in annealing zone with the variation of flow rate and aspect ratios. The result reveals that there is a decrease of temperature gradient (ΔT) as the aspect ratio increases. In terms of variance of temperature gradient (ΔT) at constant throughput, there is a meager increase for the Reynolds number less than 0.61 (≤3.6 K variance at 0.61 Re), and then the variance tends towards an asymptote as the Reynolds number goes above 1.14 (≤8.7 K variance at 2.46 Re). However, low aspect ratios (≤0.37) lead to the smaller variance of temperature gradient (ΔT) while large aspect ratios lead to higher variance of temperature gradient (ΔT) at variable throughput (≤6.9 K and ≤13.8 K variance for 0.09 and 1.5 aspect ratios respectively). Thus, it is observed that in order to minimize the temperature variance, microchannel needs to be designed with low aspect ratios (approximately $\alpha \leq 0.4$) such that the channels are smaller in depth.

4.1.6. Channel Pass Length (L_p)

The pass length of the microchannel is either shortened or lengthened to investigate the thermal gradient along the flow axis. Note that the pass lengths are varied while keeping all other geometric parameters as constant. In one heater configuration, pass length is a critical design parameter which must be specified in a way that a chosen base pair (bp) DNA fragment can be amplified at a wide range of annealing temperatures of 328–338 K. However, acceptable annealing temperature range varies depending on the melting temperature of the primers and typically, it is assumed as 5 K less than the melting temperature value.

To attain acceptable annealing temperature range (328–338 K), the thermal gradients must remain in the limit of 1.03–1.36 K/mm, 0.83–1.10 K/mm, and 0.68–0.91 K/mm for 30 mm, 37 mm, and 45 mm pass lengths respectively. In comparison with two heaters PCR chip [33], thermal gradient reduces, approximately from 4 K/mm to 1 K/mm, which helps in minimizing the major issue of thermal crosstalk (a lateral overlap of the temperature distributions) in CF-PCR chip. This demonstrates the importance of using one heater for the operation of CF-PCR chip. It is observed in Figure 8 that with the increase of Reynolds number, the variance of thermal gradient decreases which further reduces the thermal crosstalk. However, the effect of channel pass length on thermal gradient is neither linear nor consistent even at constant flow rate. Results also indicate that 37 mm pass length produces acceptable annealing temperatures with thermal gradients falling well within the desired limits, while 30 and 45 mm pass lengths produce unacceptable annealing temperatures with thermal gradients falling well below the desired limits for all Reynolds number. This suggests that lengthening and shortening of the channel pass length affects temperature gradient which could not be compensated by effective heater adjustment due to one heater chip. Thus, channel pass length is a critical microchannel design parameter, which needs to be specified in a way that the acceptable annealing temperature range is achieved.

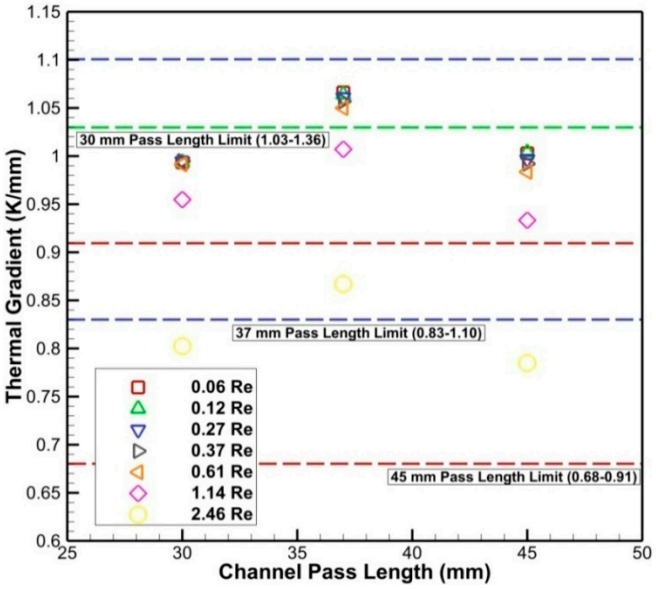

Figure 8. Effect of Reynolds number (Re) on thermal gradient (K/mm) with the variation of channel pass lengths.

4.1.7. Channel Working Region

The effect of temperature uniformity is investigated for suggesting the feasible wide range of region for microchannel location. The percentage of the feasible channel working region is the effective area of the working region divided by the total area of the working region. It is obvious that larger feasible working area will result in incorporation of more geometric flexibility within CF-PCR chip design in terms of microchannel flow length and number of cycles. It is observed in Figure 9 that the difference of temperature between center and edge of chip in transverse direction is 0.84 K, 2.11 K, and 1.48 K in denaturation, extension, and annealing zone, respectively. The temperature gradient in the transverse direction is due to lateral heat conduction and natural convection effect near the edge of the chip. The temperature distribution in the transverse direction seems to be symmetric about the center of the chip, and response starts to flatten from 8 mm onward to the center of the chip. This indicates that the temperature uniformity is established between 8 mm to 38 mm, and this is the feasible channel working region for successful implementation of PCR amplification. Overall, the one heater design offers good temperature uniformity over 66.67% area of the chip.

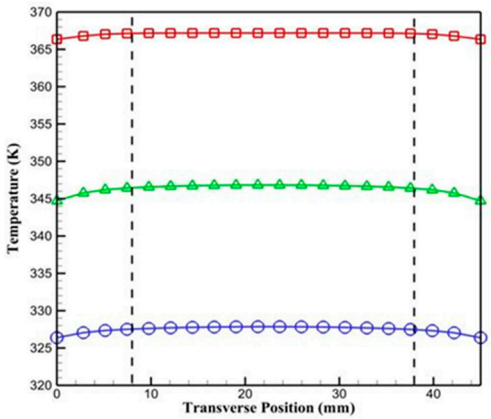

Figure 9. Variation of temperature profiles on glass surface in transverse direction.

4.2. Chip Operating Parameters

4.2.1. Flow Parameters

In case of fluid flow investigation, CF-PCR chip performance is initially gauged with the level of temperature uniformity achieved within the specific target zones. In order to identify the temperature uniformity variations within the device, the percentage of the total fluid volume within the acceptable temperature target zones (denaturation: 363–369 K, extension: 343–348 K, and annealing: 328–338 K) versus the Reynolds number is calculated and shown in Figure 10b. It is observed that the percentage decreases with the increase of Reynolds number. However, there is a steep reduction after 1.14 Re due to a large fraction of the volume in the transition zone of 338–343 K rather than the annealing temperature ranges (328–338 K) as shown in Figure 10a. Overall, it is beneficial to use a Reynolds number lower than 1.14 Re for incorporating the temperature uniformity within the device.

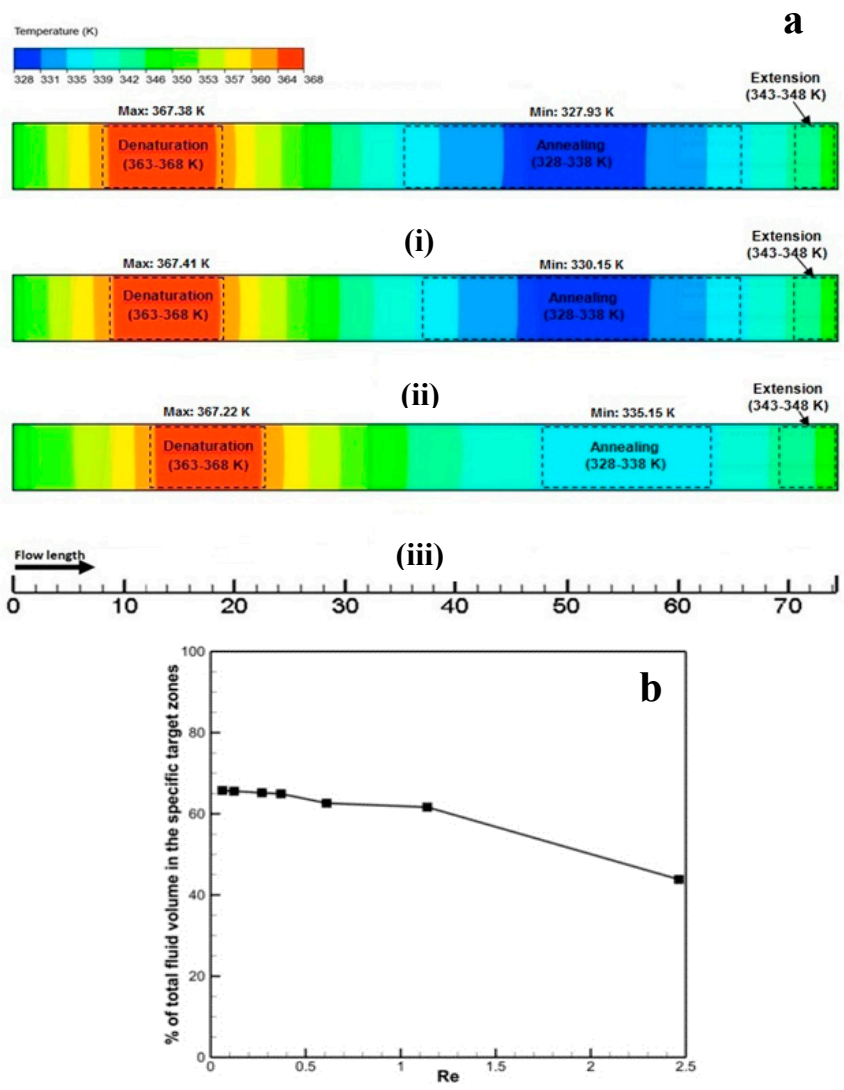

Figure 10. (**a**) Temperature distributions along the streamwise position (mm) at half the channel height (plane locates at z = 0.0375 mm): (**i**) 0.27, (**ii**) 0.61, and (**iii**) 2.46 Re; (**b**) The percentage of the total fluid volume within the acceptable temperature target zones (denaturation: 363–369 K, extension: 343–348 K, and annealing: 328–338 K) versus the Reynolds number.

4.2.2. Residence Time

Residence time is an important flow parameter which can quantify the flexibility of chip in terms of handling various size of DNA fragments. The flow regime is considered as laminar, and that exhibits the parabolic velocity profile within microchannel where maximum velocity is attained at the centerline and minimum velocity is achieved at the wall due to no-slip boundary condition. Thus, the minimum residence time is achieved by a particle which follows the centerline path. The residence time increases as a particle moves further away from centerline path and reaches infinity as it moves closer to the wall. In this study, massless fluid particles are followed using a Lagrangian particle tracking method in order to determine the residence time distributions. Once the velocity field has been computed, 1000 weightless particles that are randomly distributed over the section of themicrochannel inlet are released into the flow. Furthermore, a restitution coefficient of unity is applied to the microchannel walls. This avoids particle trajectories being trapped near the walls where the local velocity is close to zero. The residence time distribution, $E(t)$, can be computed as [34]:

$$E(t) = \frac{\Delta N_W}{N_W} \frac{1}{\Delta t} \tag{17}$$

where ΔN_W is the number of particles that have a residence time in the reactor between time t and $t + \Delta t$ each weighted by their initialvelocity normalized by the maximum velocity in the microchannel, and N_W is the total weight number of particles released in the microchannel. The residence time distribution can be easily obtained bymonitoring the particles coming out from the exit. Figure 11a shows the residence time distributions for the serpentine microchannel with the variation of Reynolds number. It is observed that as the Reynolds number increases, the spread of the RTD curves decrease due to narrowing of the velocity distribution within microchannel. Moreover, the mean residence time can be computed by averaging theresidence time of each particle. The simulated average residence times are compared to the analytical values and the numerical reaction time of 35.72 s per cycle is found out to be well within the typical error range of the experimental reaction time of 37.46 s. This shows a very good agreement to experimental result, which justifies the periodic assumption implied within the model. The particle following the centerline path is tracked to obtain the centerline residence time. Figure 11c shows the centerline temperature histories for a DNA fragment flowing through the microchannel. It is important to note that as the Reynolds number increases, the spread of temperature histories become narrow across the denaturation, annealing, and extension zones resulting in shorter residence time, while convective effects increase that result in decrease of temperature gradient (ΔT).

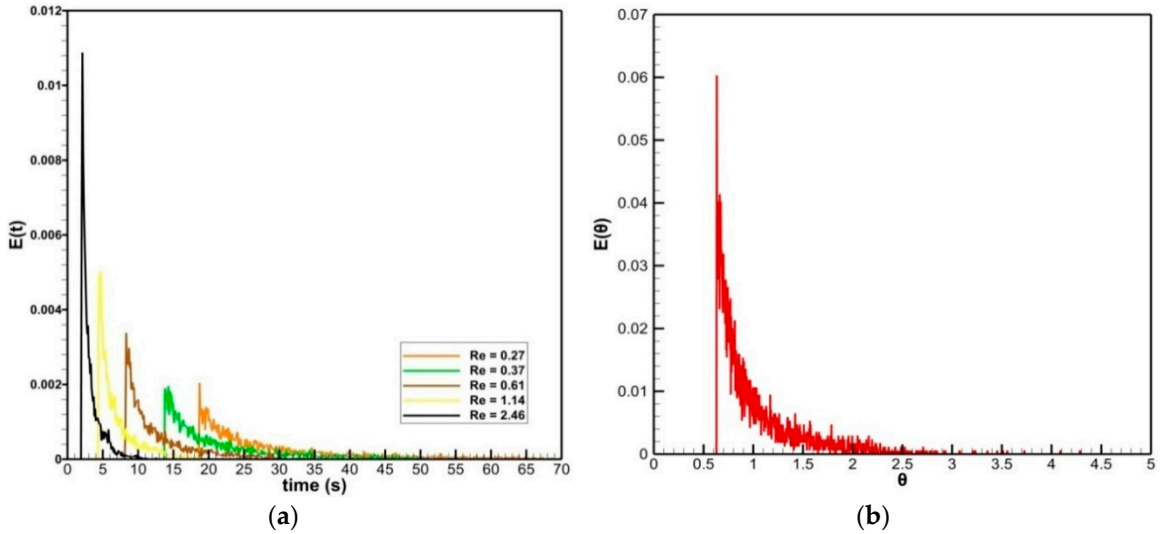

(**a**) (**b**)

Figure 11. *Cont.*

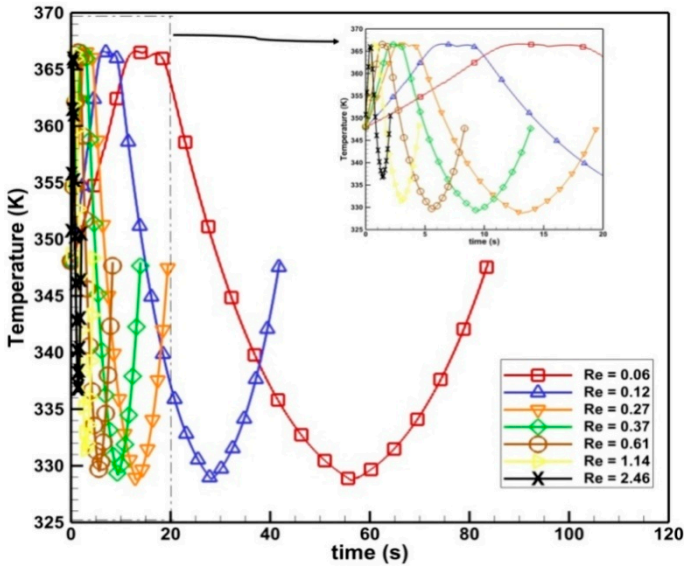

(**c**)

Figure 11. (**a**) Effect of Reynolds number (Re) on residence time distributions; (**b**) normalized residence time distribution curve for continuous-flow PCR microreactor; (**c**) centerline temperature histories for a DNA fragment flowing through the microchannel.

In general, the residence time of less than 1 s is required in both denaturation and annealing zone for each cycle. The residence time required for extension step is basically dependent on the length of base pair (bp) DNA template. Therefore, a 150 base pair (bp) DNA fragment was successfully amplified by Cao et al. [14], having residence time of 1.5 s in extension zone. In practice, DNA extension is time-limited by the Taq polymerase, whose optimal rate is about 100 bp/s. Thus, a slower heat rate (K/s) is required to obtain sufficient extension time for DNA polymerase synthesis. A 409 bp gene template, longest DNA template to be amplified in this study, requires approximately four seconds in the extension region of 343 to 348 K to successfully amplify the template, suggesting a maximum heating rate of 1.22 K/s. For the chip thermal gradient of 1.06 K/mm, the flow rate needs to be adjusted at 1.22/1.06 = 1.15 mm/s for successful amplification of a 409 bp gene template. This suggests that the heat rate requirement for any CF-PCR chip only needs to be optimized relative to the longest DNA template to be amplified. Overall, the results imply that the current design is capable of working at multiple slow heating rates which is a desirable feature to amplify various lengths of DNA base pairs. Hence, this chip design meets a critical criteria of chip flexibility.

4.2.3. Pressure Drop

In microfluidic systems, leakage occurs when pressure drop increases more than the durable bonding strength. Thus, the pressure drop is a critical flow parameter to prevent delamination of the PDMS cover sealing. The pressure drop within one-cycle model is initially calculated and then the values are multiplied by the number of cycles, which are 32 in this case. For the range of Reynolds number, the maximum pressure measured across 32 cycle PCR microdevice is 46.46 kPa (see Figure 12a). It is lower than the allowable PDMS cover bonding strength of 200 kPa [35]. Hence, this indicates that the fluid flow rate can be specified freely up to Reynolds number of 2.46 for this configuration.

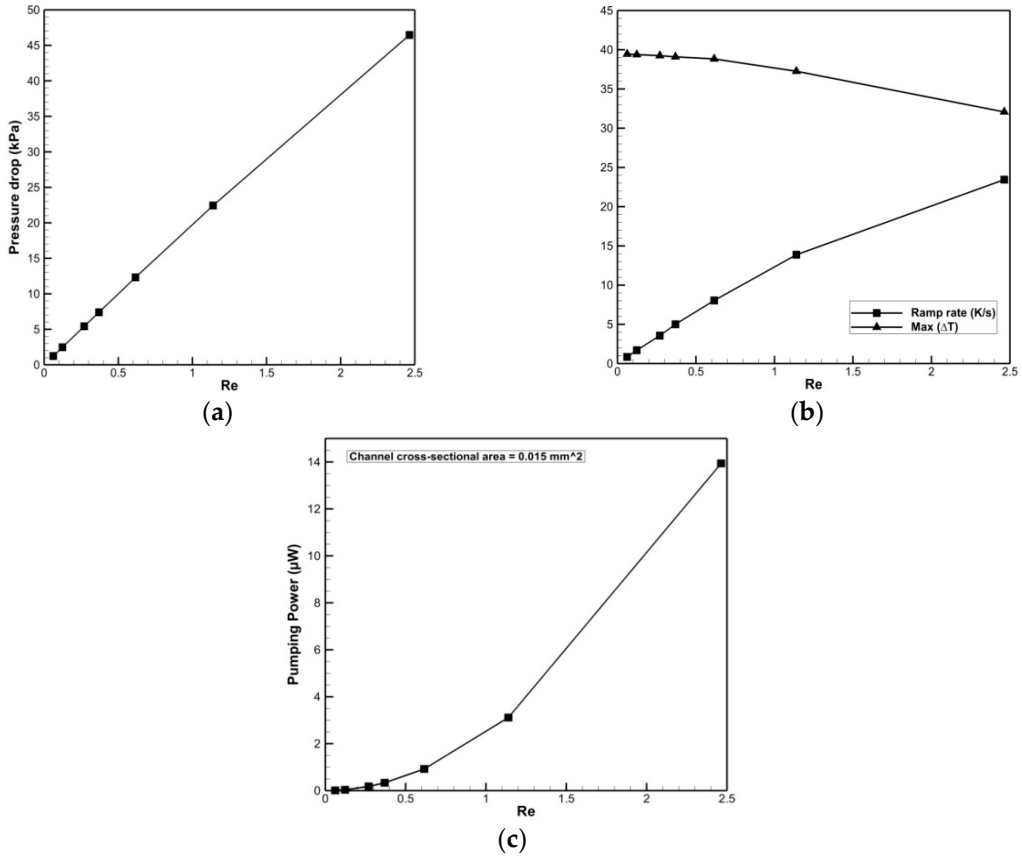

Figure 12. (**a**) Pressure drop across 32 cycle PCR microdevice with the variation of Reynolds numbers (Re); (**b**) variation of ramp rate with Reynolds number (Re); (**c**) variation of pumping power with Reynolds number (Re).

4.2.4. Ramp Rate

The ramp rate within a microchannel (Γ) is the ratio of difference between the maximum and minimum fluid temperature to the time taken in moving between that flow length (Δt).

$$\Gamma = \frac{T_{\max} - T_{\min}}{\Delta t} \tag{18}$$

It is observed in Figure 12b that with the increase of Reynolds number, the ramp rate increases with a linear trend, while maximum temperature gradient (max(ΔT)) decreases that can result in reaction failure due to non-specific PCR product formation. In comparison to three heaters configuration [35], ramp rate within a microchannel is reduced approximately by a factor of nine from 7.5 K/s to 0.85 K/s for 0.06 Re, which tackles an important issue of thermal crosstalk between the temperature zones. Overall, it is observed that the ramp rate is a critical chip performance parameter that is highly dependent on flow rate.

4.3. External Parameters

4.3.1. External Heat Transfer Coefficient ($\bar{h}$)

In general, CF-PCR chip is always exposed to air and the external heat transfer coefficient at the chip's external surface will affect the performance of the device. The objective of this study is to evaluate the effect that external heat transfer coefficient has on one heater chip. In practice, the average external heat transfer coefficient for PCR system is mostly in the range of 5–15 W/m^{2}K [23,33,36–38].

Thus, average external heat transfer coefficients of 5, 10, 12 and 15 W/m^{2}K are considered in this study. To attain an acceptable thermal profile, temperature gradient (ΔT), difference between the maximum and minimum fluid temperature for a specific channel pass length must remain well within the limit of 25–41 K to successfully amplify the DNA fragment at a wide range of annealing and denaturation limits of 328–338 K and 363–369 K, respectively.

Note that the increase of Reynolds number decreases temperature gradient, as shown in Figure 13a, due to longer rise time required by the sample to reach the desired temperature. However, the variance of ΔT at various external heat transfer coefficientsfor Reynolds number between 0.06 and 0.61 is very small (nearly 2 K). It is also observed that increasing the external heat transfer coefficient results in increase of ΔT (decrease of annealing temperature) that remains well within the requisite PCR temperatures. Additionally, there is a linear relationship between external heat transfer coefficient and ΔT. A two-fold increase in external heat transfer coefficient, from 5 to 10 W/m^{2}K, shifts ΔT upward by nearly 10 K, while a three-fold increase, from 5 to 15 W/m^{2}K, increases the ΔT by nearly 15 K. This suggests that the chip thermal profile is only shifted with the variation of external heat transfer coefficient. Critically, ΔT is well within the specific limit when Reynolds number is less than 1.14. Overall, it indicates that one heater chip is sensitive to the variation of external heat transfer coefficient and requires more stringent environment control than multiple heater PCR design.

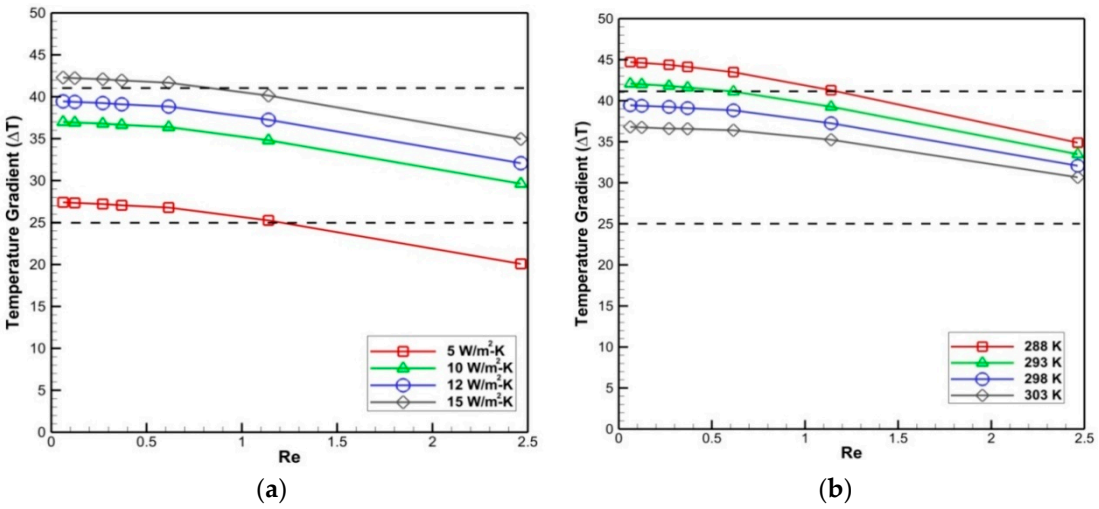

Figure 13. Effect of Reynolds number (Re) on temperature gradient (ΔT) with variation of: (**a**) external heat transfer coefficient; (**b**) ambient temperatures.

4.3.2. Ambient Temperature (T_α)

In practice, temperature stability of ambient (or room) temperature in a laboratory is vital during the in-vitro process to avoid detrimental conditions [39]. The objective of the study is to evaluate the effect ambient temperature has on one heater chip. In laboratories, hot and cold spots occur depending on the use of either heating or cooling system, which can affect the ambient temperature. Generally, most laboratories' room temperatures fluctuate between 293 and 298 K [40]. Thus, ambient temperatures of 288, 293, 298, and 303 K are considered in this study.

Note that the increase of Reynolds number decreases temperature gradient due to reduction in environmental heat losses (see Figure 13b). However, the variance of ΔT at various ambient temperatures for Reynolds number between 0.06 and 0.61 is very small (nearly 0.9 K). The chip thermal profile does not shift as much as compared to the variation of external heat transfer coefficients. It is also observed that colder ambient temperature results in increase of ΔT (decrease of annealing temperature), while hotter ambient temperature results in decrease of ΔT (increase of annealing temperature). This suggests that one heater chip needs to be operated in a stringently controlled environment. Overall, ΔT is well within the specific limit when Reynolds number is higher than 1.14. This is an important

result indicating that the ambient temperature greatly impacts the thermal profile in one heater PCR process, which can only be minimized by a stringent temperature control.

4.3.3. Pumping Power (W_{pump})

The power required to inject the fluid through syringe pump is highly dependent on pressure drop, volumetric flow rate and channel geometry. In this case, channel cross-sectional area is kept constant at 0.015 mm^2. The variation of pumping power with Reynolds number is given in Figure 12c. The pumping power increased with the increase of Reynolds number in a power-law trend. The highest pumping power is found to be 13.93 μW for 2.46 Re, which is only a fraction of total power required to perform PCR reaction. As a conclusion, pumping power seems to be the least-impact parameter of energy consumption for running the CF-PCR chip.

4.4. DNA Amplification Efficiency (λ)

The performance of CF-PCR chip is gauged in terms of DNA amplification efficiency. The PCR kinetic model proposed by Hunicke-Smith [27] is used to evaluate the DNA amplification efficiency. The concentration of S_1S_2 (double-stranded DNA (dsDNA)) in 1.14 μL volume unit cell of CF-PCR chip is shown in Figure 14a. It follows the basic principle that when S_1S_2 enters the denaturation region, S_1S_2concentration decreases due to formation of S_1 and S_2 (single-stranded DNA (ssDNA)), whereas S_1S_2 concentration increases in extension region. The logarithm of DNA amplification (AF_D) is quantified as the ratio of average S_1S_2 concentration at the outlet of each cycle to the initial S_1S_2 concentration.

$$AF_D = \log_2\left(\frac{[S_1S_2]}{[S_1S_2]_0}\right) \tag{19}$$

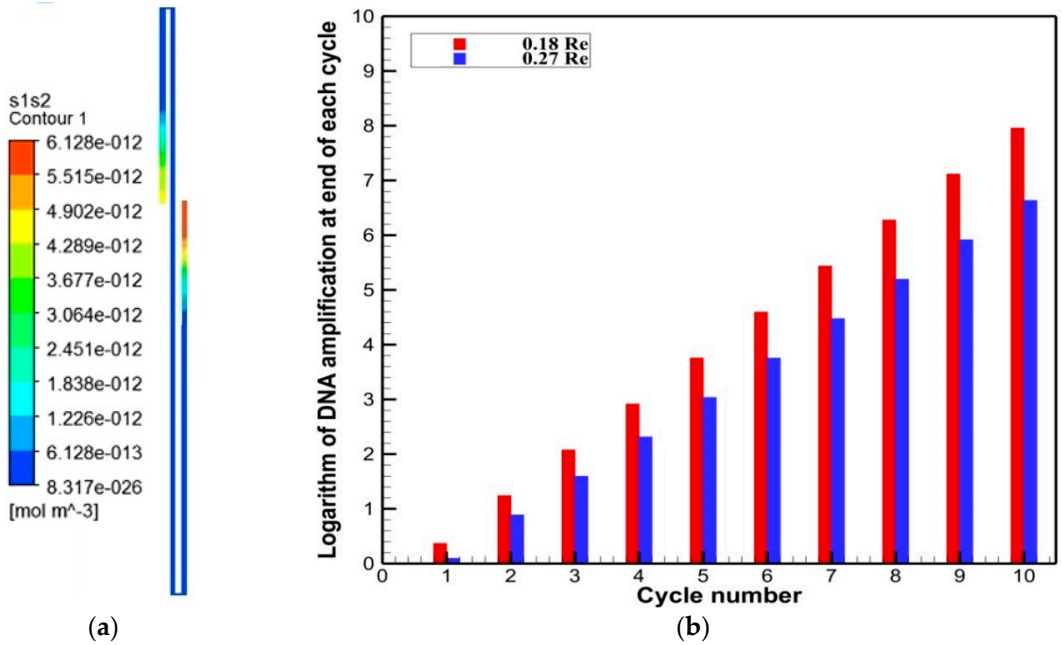

(**a**) (**b**)

Figure 14. (**a**) Concentration of S_1S_2 (double-stranded DNA (dsDNA)) in first cycle; (**b**) logarithm of DNA amplification versus the number of cycles.

The DNA amplification after 10 cycles is found out to be $2^{6.63}$ = 99.68 for nominal case, while it is $2^{7.96}$ = 249.38 for 0.18 Re (Figure 14b). This signifies that the average S_1S_2 concentration at the outlet after 10 cycles is approximately 663 and 796 times the initial concentration of S_1S_2 for nominal case and 0.18 Re respectively. However, the DNA amplification efficiency (λ) is determined by following the

basic principle of $(1 + \lambda)^n$ [27], where λ lies between 0 to 1 and n is the number of cycles. The DNA amplification efficiency (λ) is estimated to be 0.584 for nominal case, while it is 0.736 for 0.18 Re. In fact, the experimental DNA amplification efficiency for nominal case is in the range of 41–64%, which is in agreement with the numerical results that justify the kinetic parameters estimation implied within the model.

Additionally, it is also observed that there is a dependence of DNA amplification efficiency on the inlet velocity. Thus, there is a relative increase of DNA amplification efficiency by 15% at a specific lower flow rate, which signifies the importance of temperature uniformity within each zone to enhance the chip performance in terms of DNA amplification. It is therefore concluded that the most important up-front operating parameter is flow rate (or inlet velocity), which can significantly affect the device amplification efficiency.

5. Conclusions

The use of a one heater CF-PCR chip greatly simplifies the on-chip sample amplification process, which is one of the most time-consuming and labor-intensive steps in the nucleic acid analyses at the microscale level. This concept employs relatively high thermal conductivity material (invar) to create two discrete temperatures when invar sheet made partial contact with the heater and the rest of the sheet is exposed to air. A two-step three-dimensional conjugate thermal model, solid domain and one-cycle model, of a planar hybrid PDMS-glass microfluidic device employing one heater is developed. The formation patterns of the temperature gradients are numerically validated for the various protrusion lengths of the invar sheet from the heater, which showed a very good agreement with experimental data, to enable a successful temperature target zone using a single heater with reliable target specificity. Furthermore, a computational model is developed to study the effect of fourteen parameters on the thermal performance of one heater CF-PCR chip. The main conclusions based on parametric study for one heater CF-PCR chip are summarized as below:

1. The influence of various substrate-cover materials on the one heater CF-PCR chip are examined and the results show that low thermal conductive material, PDMS, seems to be an acceptable option as a one heater chip cover only due to minimization of natural convection effects, while high thermal conductive material, silicon, minimizes the chip-wide temperature variance which yieldsundesired thermal profile. Overall, glass or glass-PDMS seems to be an excellent substrate-cover material choice for one heater chip which can lead to the additional benefits of low-cost and commercially viable point-of-care diagnostics.

2. In terms of influence of various substrate thicknesses, it was found that the variation of metal alloy thickness adversely affects the thermal profile. Thicker metal alloy assisted chips (>0.5 mm) result in unreasonable chip-wide temperature variance due to relative enhancement of heat rates across the annealing and extension zones. Thus, thinner metal alloy assisted chips are recommended in the absence of other design constraints.

3. The analysis of chip design parameters shows that short channel spacings (≤1 mm) and low aspect ratios ($\alpha \leq 0.4$) need to be considered to attain desirable PCR thermal profile with one heater chip. For channel pass length, lengthening and shortening of the microchannel affects temperature gradient which could not be compensated by effective heater adjustment due to one heater chip. This suggests that channel pass length is one of the most critical microchannel design parameters, which needs to be specified in a way that the acceptable annealing temperature range is achieved.

4. In terms of chip operating parameters, the flow rate (or Reynolds number) seems to be the most important up-front operating parameter that needs to be considered at the time of design to meet the desired thermocycling protocol requirements. In order to obtain optimum chip thermal performance and DNA amplification efficiency, one heater chip is recommended to be operated at flow rates of ≤0.37 Re to minimize the impact of various parameters on chip performance.

5. It is also found out that the external parameters, such as external heat transfer coefficient and ambient temperature, only shift thermal profile, which could not be overcome by heater adjustment

due to one heater design. This indicates that in case of one heater chip, environment conditions need to be stringently controlled and monitored to perform PCR process.

Moreover, this work has led to the thermal and fluidic characterization of one heater CF-PCR chip in an accurate manner, which pinpoints the several critical parameters, such as substrate material, substrate thickness, channel spacing, channel pass length, aspect ratio, flow rate, and external parameters, that can either improve or deteriorate the chip performance. Finally, the chip flexibility, thermal crosstalk reduction, and low-cost substrate option indicate attractive prospects for practical implementation of one heater CF-PCR chip. Further work will be to include thermal and flow performance of non-Newtonian fluid in CF-PCR chip. In addition, cycle time needs to be reduced by narrowing the channel between denaturation and annealing zone to enable rapid DNA amplification. It can be more effective to consider both non-Newtonian fluid flow and the geometric optimization of microchannel in the future.

Author Contributions: Conceptualization, U.P. and I.A.; Methodology, U.P.; Software, U.P.; Validation, U.P.; Formal Analysis, F.A.; Investigation, I.A.; Resources, F.A.; Data Curation, M.R.K.; Writing—Original Draft Preparation, U.P.; Writing—Review & Editing, F.A.; Visualization, M.R.K.; Supervision, F.A.; Project Administration, U.P.

Funding: This research received no external funding.

Conflicts of Interest: The authors declare no conflict of interest.

References

1. Mullis, K.; Faloona, F.; Scharf, S.; Saiki, R.K.; Horn, G.T.; Erlich, H. Specific enzymatic amplification of DNA in vitro: The polymerase chain reaction. *Cold Spring Harbor Symp. Quant. Biol.* **1986**, *51*, 263–284. [CrossRef] [PubMed]
2. Chiavazzo, E.; Gear, C.W.; Dsilva, C.J.; Rabin, N.; Kevrekidis, I.G. Reduced models in chemical kinetics via nonlinear data-mining. *Processes* **2014**, *2*, 112–140. [CrossRef]
3. Yang, S.; Kiang, S.; Farzan, P.; Ierapetritou, M. Optimization of reaction selectivity using CFD-based compartmental modeling and surrogate-based optimization. *Processes* **2019**, *7*, 9. [CrossRef]
4. Baah Appiah-Nkansah, N.; Li, J.; Zhang, K.; Zhang, M.; Wang, D. Study on mass transfer kinetics of sugar extraction from sweet sorghum biomass via diffusion process and ethanol yield using SSF. *Processes* **2019**, *7*, 137. [CrossRef]
5. Chen, J.; Song, W.; Xu, D. Computational fluid dynamics modeling of the catalytic partial oxidation of methane in microchannel reactors for synthesis gas production. *Processes* **2018**, *6*, 83. [CrossRef]
6. Benamara, N.; Assoua, D.; Jaffeux, L.; Vanoye, L.; Simescu-Lazar, F.; Zanota, M.-L.; Bornette, F.; Meille, V.; Pitault, I. A new concept of stirred multiphase reactor using a stationary catalytic foam. *Processes* **2018**, *6*, 117. [CrossRef]
7. Kim, S.W. Effect of particle size on carbon nanotube aggregates behavior in dilute phase of a fluidized bed. *Processes* **2018**, *6*, 121. [CrossRef]
8. Mattei, G.; Giusti, S.; Ahluwalia, A. Design criteria for generating physiologically relevant in vitro models in bioreactors. *Processes* **2014**, *2*, 548–569. [CrossRef]
9. Hakat, Y.; Kotbagi, T.V.; Bakker, M.G. Ag/SiO_2- and Ag/Co_3O_4-based monolithic flow microreactors for hydrogenation of dyes: Their activity and stability. *Processes* **2015**, *3*, 98–112. [CrossRef]
10. Cinquemani, E. Identifiability and reconstruction of biochemical reaction networks from population snapshot data. *Processes* **2018**, *6*, 136. [CrossRef]
11. Hashimoto, M.; Chen, P.C.; Mitchell, M.W.; Nikitopoulos, D.E.; Soper, S.A.; Murphy, M.C. Rapid PCR in a continuous flow device. *Lab Chip* **2004**, *4*, 638–645. [CrossRef] [PubMed]
12. Mohr, S.; Zhang, Y.H.; MacAskill, A.; Day, P.J.R.; Barber, R.W.; Goddard, N.J.; Emerson, D.R.; Fielden, P.R. Numerical and experimental study of a droplet-based PCR chip. *Microfluid. Nanofluid.* **2007**, *3*, 611–621. [CrossRef]
13. Crews, N.; Ameel, T.; Wittwer, C.; Gale, B. Flow-induced thermal effects on spatial DNA melting. *Lab Chip* **2008**, *8*, 1922–1929. [CrossRef]
14. Cao, Q.; Kim, M.C.; Klapperich, C. Plastic microfluidic chip for continuous-flow polymerase chain reaction: Simulations and experiments. *Biotechnol. J.* **2011**, *6*, 177–184. [CrossRef]

15. Sun, K.; Yamaguchi, A.; Ishida, Y.; Matsuo, S.; Misawa, H. A heater-integrated transparent microchannel chip for continuous-flow PCR. *Sens. Actuators B Chem.* **2002**, *84*, 283–289. [CrossRef]
16. Kuan, I.; Gu, W.; Wu, J.; Wei, C.; Chen, K.; Yu, C. Effects of grafting poly(ethyleneoxide) on the amplification efficiency of a poly(dimethylsiloxane)-based flow-through PCR device. *Chem. Eng. J.* **2008**, *143*, 326–330. [CrossRef]
17. Nakayama, T.; Hiep, H.M.; Furui, S.; Yonezawa, Y.; Saito, M.; Takamura, Y.; Tamiya, E. An optimal design method for preventing air bubbles in high-temperature microfluidic devices. *Anal. Bioanal. Chem.* **2010**, *396*, 457. [CrossRef]
18. Cao, Q.; Mahalanabis, M.; Chang, J.; Carey, B.; Hsieh, C.; Stanley, A.; Odell, C.A.; Mitchell, P.; Feldman, J.; Pollock, N.R.; et al. Microfluidic chip for molecular amplification of influenza ARNA in human respiratory specimens. *PLoS ONE* **2012**, *7*, e33176. [CrossRef]
19. Wu, W.; Lee, N.Y. Three-dimensional on-chip continuous-flow polymerase chain reaction employing a single heater. *Anal. Bioanal. Chem.* **2011**, *400*, 2053–2060. [CrossRef]
20. Wu, W.; Lee, N.Y. Flow-through PCR on a 3D qiandu-shaped polydimethylsiloxane (PDMS) microdevice employing a single heater: Toward microscale multiplex PCR. *Analyst* **2012**, *137*, 2069–2076. [CrossRef]
21. Wu, W.; Lee, N.Y. Bent polydimethylsiloxane–polycarbonate hybrid microdevice for on-chip flow-through polymerase chain reaction employing a single heater. *Microchim. Acta.* **2014**, *181*, 1697–1705.
22. Trinh, K.T.L.; Wu, W.; Lee, N.Y. Planar poly(dimethylsiloxane) (PDMS)–glass hybrid microdevice for a flow-through polymerase chain reaction (PCR) employing a single heater assisted by an intermediate metal alloy layer for temperature gradient formation. *Sens. Actuators B* **2014**, *190*, 177–184. [CrossRef]
23. Chen, J.J.; Liao, M.H.; Li, K.T.; Shen, C.M. One-heater flow-through polymerase chain reaction device by heat pipes cooling. *Biomicrofluidics* **2015**, *9*, 014107. [CrossRef] [PubMed]
24. Incropera, F.P.; Lavine, A.S.; Bergman, T.L.; DeWitt, D.P. *Fundamentals of Heat and Mass Transfer*; Wiley: New York, NY, USA, 2002.
25. *ANSYS*; release15.0; ANSYS Inc.: Canonsburg, PA, USA, 2013.
26. Erlich, H.A.; Freeman, W.H. *PCR Technology: Principles and Applications for DNA Amplification*; Freeman and Company: New York, NY, USA, 1992.
27. Hunicke-Smith, S.P. PCR and cycle sequencing reactions: A new device and engineering model. Ph.D. Thesis, Stanford University, Stanford, CA, USA, 1997.
28. Mehra, S.; Hu, W. A kinetic model of quantitative real-time polymerase chain reaction. *Biotechnol. Bioeng.* **2005**, *91*, 848–860. [CrossRef]
29. Priye, A.; Hassan, Y.A.; Ugaz, V.M. Microscale chaotic advection enables robust convective DNA replication. *Anal. Chem.* **2013**, *85*, 10536–10541. [CrossRef]
30. Wang, Y.; Pant, K.; Grover, J.; Sundaram, S. Multiphysics simulational analysis of a novel PCR micro-device. *Nanotech* **2007**, *3*, 456–459.
31. Lima, R.; Wada, S.; Tanaka, S.; Takeda, M.; Ishikawa, T.; Tsubota, K.I.; Imai, Y.; Yamaguchi, T. In vitro blood flow in a rectangular PDMS microchannel: Experimental observations using a confocal micro-PIV system. *Biomed. Microdevices* **2008**, *10*, 153–167. [CrossRef]
32. Mohammadi, M.; Jovanovic, G.N.; Sharp, K.V. Numerical study of flow uniformity and pressure characteristics with in a microchannel array with triangular manifolds. *Comput. Chem. Eng.* **2013**, *52*, 134–144. [CrossRef]
33. Thomas, S.; Orozco, R.L.; Ameel, T. Thermal gradient continuous-flow PCR: A guide to design. *Microfluid. Nanofluid.* **2014**, *17*, 1039–1051. [CrossRef]
34. Fogler, H.S. *Elements of Chemical Reaction Engineering*, 2nd ed.; PTR Prentice Hall: Englewood Cliffs, NJ, USA, 1992.
35. Kumar, S.; Cartas-Ayala, M.A.; Thorsen, T. Thermal modeling and design analysis of a continuous flow microfluidic chip. *Int. J. Therm. Sci.* **2013**, *67*, 72–86. [CrossRef]
36. Zhang, Q.; Wang, W.; Zhang, H.; Wang, Y. Temperature analysis of continuous-flow micro-PCR based on FEA. *Sens. Actuators B* **2002**, *82*, 75–81. [CrossRef]
37. Chen, P.C.; Fan, W.; Hoo, T.K.; Chan, L.C.Z.; Wang, Z. Simulation guided-design of a microfluidic thermal reactor for polymerase chain reaction. *Chem. Eng. Res. Des.* **2012**, *90*, 591–599. [CrossRef]
38. Moschou, D.; Vourdas, N.; Kokkoris, G.; Papadakis, G.; Parthenios, J.; Chatzandroulis, S.; Tserepi, A. All-plastic, low-power, disposable, continuous-flow PCR chip with integrated microheaters for rapid DNA amplification. *Sens. Actuators B* **2014**, *199*, 470–478. [CrossRef]

39. Butler, J.M.; Johnson, J.E.; Boone, W.R. The heat is on: Room temperature affects laboratory equipment—An observational study. *J. Assist. Reprod. Genet.* **2013**, *30*, 1389–1393. [CrossRef]
40. Bove, R. Temperature measurement in the clinical laboratory. Good isn't good enough. *Med. Lab. Obs.* **2011**, *43*, 36–39.